nature medicine

Multiplexed ion beam imaging of human breast tumors

Michael Angelo[1,2], Sean C Bendall[1], Rachel Finck[1], Matthew B Hale[1], Chuck Hitzman[3], Alexander D Borowsky[4], Richard M Levenson[4], John B Lowe[5], Scot D Liu[5], Shuchun Zhao[6], Yasodha Natkunam[6] & Garry P Nolan[1]

Immunohistochemistry (IHC) is a tool for visualizing protein expression that is employed as part of the diagnostic workup for the majority of solid tissue malignancies. Existing IHC methods use antibodies tagged with fluorophores or enzyme reporters that generate colored pigments. Because these reporters exhibit spectral and spatial overlap when used simultaneously, multiplexed IHC is not routinely used in clinical settings. We have developed a method that uses secondary ion mass spectrometry to image antibodies tagged with isotopically pure elemental metal reporters. Multiplexed ion beam imaging (MIBI) is capable of analyzing up to 100 targets simultaneously over a five-log dynamic range. Here, we used MIBI to analyze formalin-fixed, paraffin-embedded human breast tumor tissue sections stained with ten labels simultaneously. The resulting data suggest that MIBI can provide new insights into disease pathogenesis that will be valuable for basic research, drug discovery and clinical diagnostics.

Antibodies were first employed in tissue section analysis in 1942 to visualize pneumococcal antigens in organ biopsies from mice infused with live bacteria[1]. Since that time, IHC has become a mainstay of clinical diagnostics and basic research and is primarily used to assess the spatial distribution of one or two (rarely more) antigens in tissue sections. Despite the high specificity of many antibodies, the concentration of most antigens is insufficient to permit detection by conventional assays without signal amplification[2–4]. Signal amplification is typically achieved by using multivalent enzyme-linked secondary antibodies that bind the Fc portion of the primary antibody. In brightfield microscopy, the most commonly used enzymatic reporter is horseradish peroxidase, typically used to oxidize 3,3′-diaminobenzidine (DAB), resulting in accumulation of a brown precipitate. Such nonlinear enzymatic amplification can result in poor correlation with the target antigen concentration[2,5].

Simultaneous detection of multiple antigens is subject to additional constraints that limit the utility of existing IHC-based analysis for predictive biomarker development in human clinical trials and clinical diagnostics. Colorimetric detection of four antigens has been reported using multiple enzyme-linked secondary antibodies, but in practice, this approach is usually limited to two because of difficulties encountered in sample preparation and imaging[2,6]. Fluorescent labels used in the related immunofluorescence technique provide a higher signal-to-noise ratio and are more frequently used for simultaneous detection of multiple targets. Practical limitations include the need for primary antibodies generated in dissimilar host species and for nonoverlapping reporter emission spectra[5]. Thus, conventional IHC or immunofluorescence methodologies do not support the robust generation of quantitative multiplexed data needed to understand the relationship between tissue microarchitecture and expression at a subcellular level.

Previous work by our lab and others has demonstrated the utility of elemental mass spectrometry in circumventing similar limitations encountered in fluorescence-based flow cytometry[7–11]. In this approach, termed mass cytometry, cells stained with antibodies carrying isotopically pure nonbiological elemental metal reporters are nebulized into single-cell droplets before sequential analysis via inductively coupled plasma time-of-flight mass spectrometry. In principle, single-cell analysis of up to 100 parameters can be achieved without spectral overlap between channels[11].

Here, we present a modality that uses secondary ion mass spectrometry to image metal isotope–carrying antibodies. MIBI is capable of analyzing samples stained simultaneously with up to 100 metal isotope–labeled antibodies and is compatible with standard formalin-fixed, paraffin-embedded (FFPE) tissue sections, the most common type of specimen in clinical repositories worldwide[12]. Depending on the element of interest, MIBI can achieve as low as parts-per-billion sensitivity over a five-log dynamic range at resolutions comparable to those achieved with high-magnification light microscopy[13–16]. We used MIBI to image breast tumor tissue sections stained with clinically relevant metal-conjugated antibodies. The data generated from these experiments can be interpreted within a conventional imaging context and by using high-dimensional analytics that reveal hidden phenotypic and morphological features of each biopsy.

RESULTS

Performance assessment of MIBI

The workflow for MIBI is comparable to that of immunofluorescence and IHC assays (**Fig. 1**). Instead of fluorophores or enzyme-conjugated

[1]Baxter Laboratory in Stem Cell Biology, Department of Microbiology and Immunology, Stanford University, Stanford, California, USA. [2]Department of Laboratory Medicine, University of California–San Francisco, San Francisco, California, USA. [3]Department of Materials Science and Engineering, Stanford University, Stanford, California, USA. [4]Department of Pathology and Laboratory Medicine, University of California–Davis, Health System, Sacramento, California, USA. [5]Department of Pathology, Genentech, South San Francisco, California, USA. [6]Department of Pathology, Stanford University, Stanford, California, USA. Correspondence should be addressed to G.P.N. (gnolan@stanford.edu).

Received 13 May 2013; accepted 17 December 2013; published online 2 March 2014; doi:10.1038/nm.3488

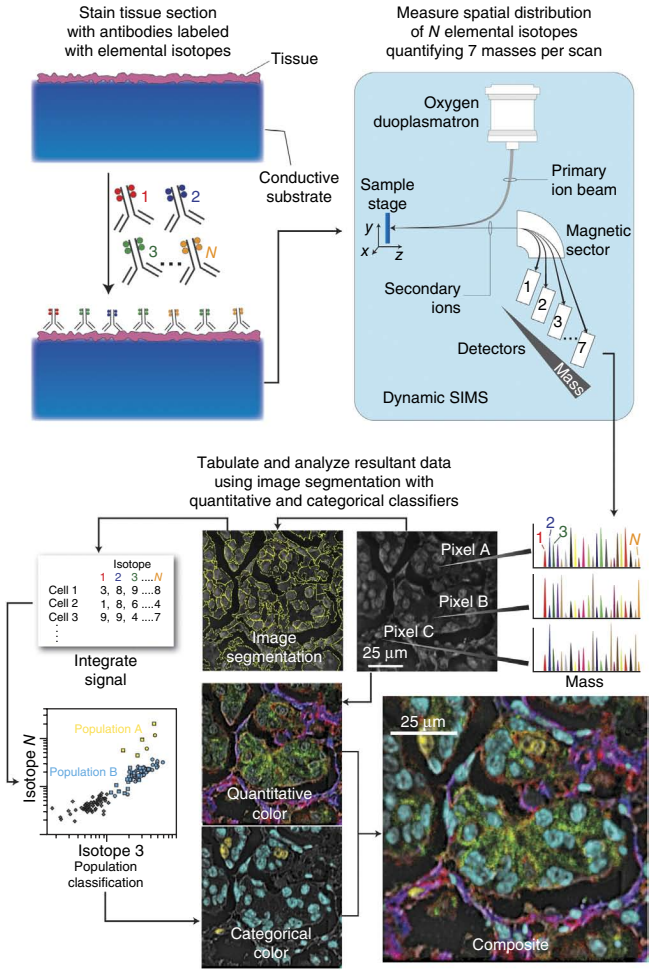

Figure 1 Workflow summary of MIBI. Biological specimens, such as FFPE tissue or cell suspensions, are immobilized on a conductive substrate, such as indium tin oxide–coated glass or silicon wafer. Samples are subsequently stained with antibodies conjugated to unique transition element isotope reporters, dried and loaded under vacuum for MIBI analysis. The sample surface is rasterized with an oxygen primary ion beam that sputters the antibody-specific isotope reporters native to the sample surface as secondary ions. Metal-conjugated antibodies are quantified via replicate scans of the same field of view, where up to seven metal reporters are measured with each scan, and the detectors are mass calibrated after each scan cycle. ROIs demarcating nuclear and cytosolic compartments of each cell are integrated, tabulated and categorized. Composite images comprised of pseudocolored categorical features and quantitative three-color overlays are constructed to summarize multidimensional expression data.

reagents, biological specimens are incubated with primary antibodies coupled to stable lanthanides that are highly enriched for a single isotope (**Fig. 1**). Primary antibodies are combined in solution for simultaneous incubation with the specimen. The specimens prepared for MIBI are mounted in a sample holder and subjected to a rasterized oxygen duoplasmatron primary ion beam. As this ion beam strikes the sample, lanthanide adducts of the bound antibodies are liberated as secondary ions. In this study, we subsequently analyzed the secondary ions via a magnetic sector mass spectrometer equipped with multiple detectors, permitting parallel detection of multiple lanthanide isotopes (mass-based reporters). The resultant data produced a two-dimensional map of the elemental distribution of each lanthanide and thus each antibody and its corresponding epitope.

As part of preliminary validation studies, we assessed peripheral blood mononuclear cells (PBMCs) stained with seven metal isotope–conjugated primary antibodies to CD3, CD4, CD8, CD14, CD19, CD45 and human leukocyte antigen–DR (HLA-DR) in parallel using mass cytometry and MIBI (**Fig. 2**). We performed mass cytometry on the PBMC suspension as described previously[7]. For MIBI, cells were immobilized on a poly-L-lysine–coated silicon wafer, dried under vacuum and subsequently analyzed using a NanoSIMS 50L mass spectrometer. Sequential 50-µm fields were each scanned for 5 min (**Fig. 2a**). We aligned 10-µm overlapping regions of each field to construct a composite mosaic using an automated script in Matlab. We segmented the resultant mosaic into single-cell regions of interest (ROIs) using the CD45 channel[17]. To extract single-cell expression data for each antibody, the ion count for each channel was integrated for each cell ROI. To achieve this mosaic, we imaged 1,200 fields for 5 min per field (99 h total scan time). However, as discussed below, orders-of-magnitude improvements in throughput can be achieved with appropriate sample preparation and instrumentation modifications.

Mass cytometry and MIBI produced comparable results and qualitative patterns of expression when analyzed via traditional biaxial plots (**Fig. 2b**), with marker intensities determined by MIBI demonstrating a linear dynamic range spanning five orders of magnitude. Additionally, both platforms yielded quantitatively similar frequencies for seven manually gated cell populations (**Fig. 2c**), with three of these populations differing by less than 1% between platforms (B cells, $CD8^+$ T cells and $CD4^+$ T cells). Altogether, using PBMCs as a test case, MIBI yielded results both qualitatively and quantitatively equivalent to those of a conventional analytical platform and also revealed spatial features of protein expression at the subcellular level.

Ten-color imaging of human breast tumor tissue sections

In order to use MIBI for analysis of tissue sections acquired in a diagnostic setting, we sought to verify the performance of metal-conjugated versions of the antibodies by comparing the staining behavior of metal-conjugated versus unmodified primary antibodies using conventional immunoperoxidase chemistry. Secondary staining of serial sections from a single FFPE human breast tumor tissue block treated with metal-conjugated or unmodified primary antibodies for Ki-67 or estrogen receptor-α (ERα) demonstrated positive nuclear staining of comparable intensity and similar levels of background staining (**Fig. 3a**), indicating that the metal conjugation did not materially affect specific and nonspecific staining behavior.

Finally, to assess the overall performance of MIBI in a diagnostic imaging application, we analyzed FFPE breast tumor tissue sections with different immunophenotypic profiles. We verified ERα, progesterone receptor (PR) and human epidermal growth factor receptor-2 (HER2) positivity in a clinical IHC lab using validated reagents. For MIBI, we mounted tumor sections on poly-L-lysine–coated silicon wafers, deparaffinized them and subjected them to heat-induced epitope retrieval before overnight staining with metal-conjugated antibodies for double-stranded DNA (dsDNA), ERα, PR, E-cadherin, Ki-67, vimentin, actin, keratin and HER2. Conveniently, a hematoxylin counterstain can be readily detected by measuring its elemental aluminum content. The following day, the sections were washed, counterstained with hematoxylin and dehydrated via graded ethanol series.

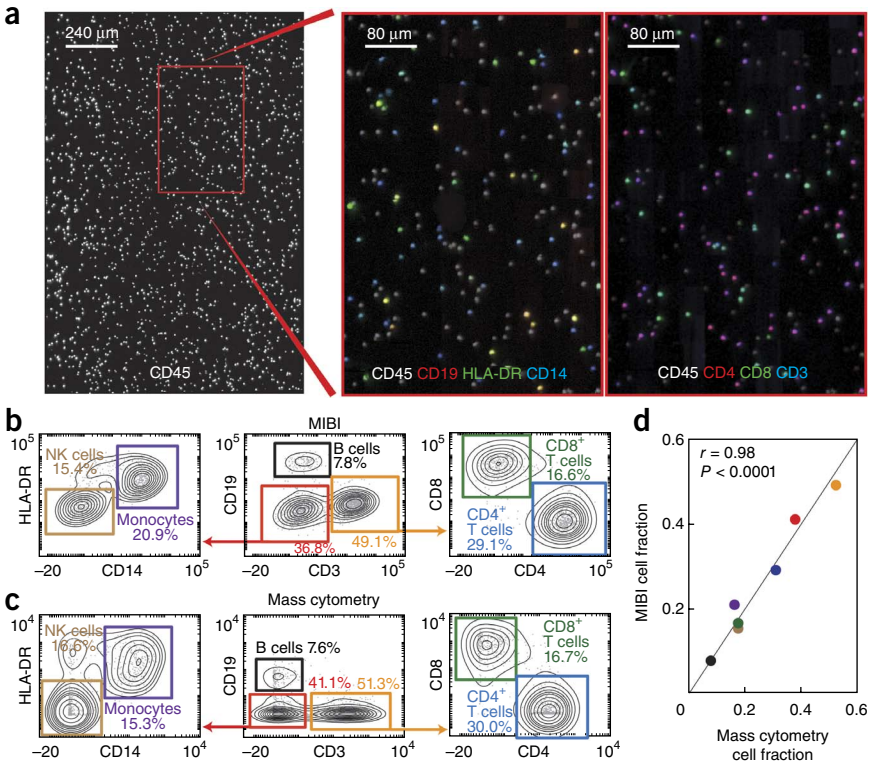

Figure 2 Analysis of PBMCs stained with metal-conjugated antibodies using mass cytometry and MIBI. (**a**) MIBI analysis of PBMCs stained with seven antibodies and immobilized on a silicon wafer. The signal intensity of the metal label for each respective antibody within each cell is illustrated in a mosaic composed of 1,200 separately acquired 50-μm fields of view. Data are representative of three replicate experiments. (**b**,**c**) Hierarchical gating and comparison of seven cell populations identified using mass cytometry or MIBI. Biaxial plots are arcsinh(*x*/5) scaled. NK, natural killer. (**d**) Pearson correlation of the relative abundance of each cell population between the two methods ($r = 0.98$, $P < 0.0001$, two-tailed Student's *t*-test).

Using the MIBI analysis, conventional high-resolution images can be generated using FFPE tissues. We acquired ten-marker images in two consecutive scans of the same 80-μm field of view, with each scan lasting 25 min. We acquired images for hematoxylin, ERα, PR, Ki-67, E-cadherin, HER2 and dsDNA during the first scan and keratin, vimentin and actin during the second. We constructed pseudobrightfield images mimicking traditional DAB staining by coding hematoxylin on a white-to-blue scale and putting the desired marker on a white-to-brown scale (**Fig. 3b**). We also constructed pseudofluorescence images mimicking three-color immunofluorescence using a dsDNA channel (red), a hematoxylin channel (blue) and a marker channel (green) (**Fig. 3b**). Pseudobrightfield and pseudofluorescence composites for each antibody within a single field of view for three tumor biopsies are shown in **Figure 3c**. Comparison of HER2, ERα and PR positivity across the three specimens demonstrated appropriate expression of each marker with respect to immunophenotypes established by conventional IHC staining. Sections expressing ERα and PR demonstrated well-demarcated nuclear staining, scattered Ki-67$^+$ nuclei and intense positive staining for vimentin in mesenchymal cells. HER2$^+$ sections demonstrated strong membrane staining. E-cadherin, actin and keratin also demonstrated appropriate subcellular staining patterns.

Image segmentation and feature extraction

In order to further explore the utility of the information inherent in the quantitatively multiplexed images in this study, we performed image segmentation so that cellular features could be analyzed and compared. We segmented hematoxylin and dsDNA channels for each tumor using CellProfiler in order to extract summary statistics describing subcellular expression[18,19] (**Fig. 4a**). The pixel intensity for each marker and subcellular ROI demonstrated distinctly different distributions with respect to the known immunophenotype of each tumor (**Supplementary Fig. 1**). We quantified mean pixel intensities for each marker within nuclear, cytoplasmic and cellular ROIs for each cell. Biaxial scatter plots demonstrated marker coexpression matching the known immunophenotype for each tumor (**Fig. 4b**). ERα$^+$PR$^+$HER2$^+$ and ERα$^+$PR$^+$ tumors demonstrated appropriate nuclear coexpression of ERα and PR that was absent in the ERα$^-$PR$^-$HER2$^+$ tumor. Subpopulations of keratin$^+$ and E-cadherin$^+$ ductal cells were distinctly segregated from vimentin$^+$ mesenchymal cells.

We further assessed quantitative accuracy by comparing MIBI to a US Food and Drug Administration (FDA)-approved quantitative image analysis (QIA) workflow for determining the staining intensity of scanned IHC tissue sections. We used QIA to quantify ERα nuclear expression in a cohort of nine breast tumors. We manually annotated tumor-containing regions and subsequently analyzed them using an automated algorithm optimized for determining immunoperoxidase nuclear staining intensity. The resultant data included mean intensity and an overall H-score (a scale for quantifying the intensity of expression of a protein in IHC staining). Linear regression analysis comparing mean ERα nuclear staining intensity by MIBI or IHC demonstrated robust agreement between the two methods (**Fig. 4c**, $r = 0.99$, $P < 0.00001$). We calculated cutoff points for MIBI staining intensity with the resultant linear equation (MIBI = 0.064 + 0.0073 × IHC) using the respective values for negative, 1+, 2+ and 3+ employed by QIA; we subsequently used these cutoff points to calculate an overall H-score. Linear regression analysis comparing IHC and MIBI H-scores also demonstrated strong robust agreement (**Fig. 4c**, $r = 0.99$, $P < 0.00001$) with a slope near unity ($m = 1.06 \pm 0.06$ s.d.). The strong correlation between H-scores derived from each method suggests that MIBI not only captured the mean overall staining intensity but also was able to accurately capture the biological variability of ERα expression. This implies that the true distribution of staining intensity was valid and accurately recapitulated. These results also suggest that, at least within the context of its application here, MIBI analysis is not materially affected by sample-to-sample matrix effects that can arise when using a bioanalysis platform. Furthermore, comparison of ERα staining intensity in serial sections treated with all nine antibodies or only the ERα-specific antibody shows that the quantitative accuracy of this method is unaffected by multiplexing (**Supplementary Fig. 2**).

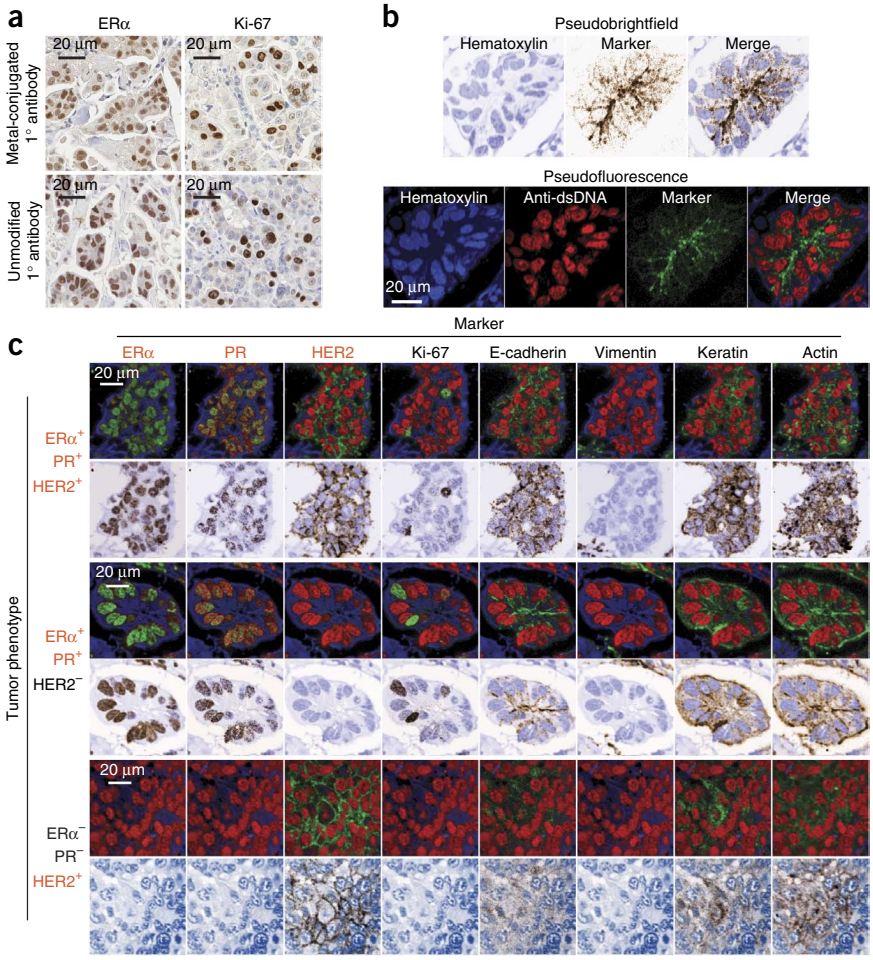

Figure 3 Ten-color imaging of human breast tumors using MIBI. (**a**) Performance assessment of metal-conjugated antibodies using immunoperoxidase staining. Representative fields of serial sections from a single breast tumor biopsy stained with either conjugated or unconjugated primary antibodies to Ki-67 or ERα are shown. Staining was performed on serial sections from three different breast tumor biopsies. (**b**) Visual representation of MIBI data. Pseudobrightfield or pseudoimmunofluorescence image reconstructions are derived from single-channel ion data for hematoxylin, dsDNA and the marker of interest. (**c**) MIBI of FFPE tissue sections from three different patients. Expression of HER2, ERα and PR by MIBI matches the immunophenotype of each specimen determined using clinically validated immunoperoxidase staining. ERα, PR and Ki-67 exhibit nuclear localization, and expression of E-cadherin, actin, HER2 and keratin is membranous or cytoplasmic. In total, twelve different breast tumor biopsies were analyzed with at least three replicate samples. At least five fields of view were acquired for each replicate. Field of view, 80 μm.

Integrated histologic and immunophenotypic features of multidimensional MIBI data can be visualized by generating composite images that combine quantitative (continuous) cytoplasmic and categorical (positive or negative) nuclear expression patterns (**Fig. 5**). Hormone receptor–positive regions within the epithelial compartment, showing variable non-nuclear expression of actin and E-cadherin, can be distinguished from interspersed mesenchymal cells coexpressing actin and vimentin. Approximately 8% of cells were seen to be Ki-67$^+$. Unlike conventional chromogenic IHC, which is not well suited to detecting colocalization of multiple markers, MIBI analysis readily demonstrates ERα$^+$PR$^+$ or ERα$^+$PR$^+$Ki-67$^+$ subpopulations.

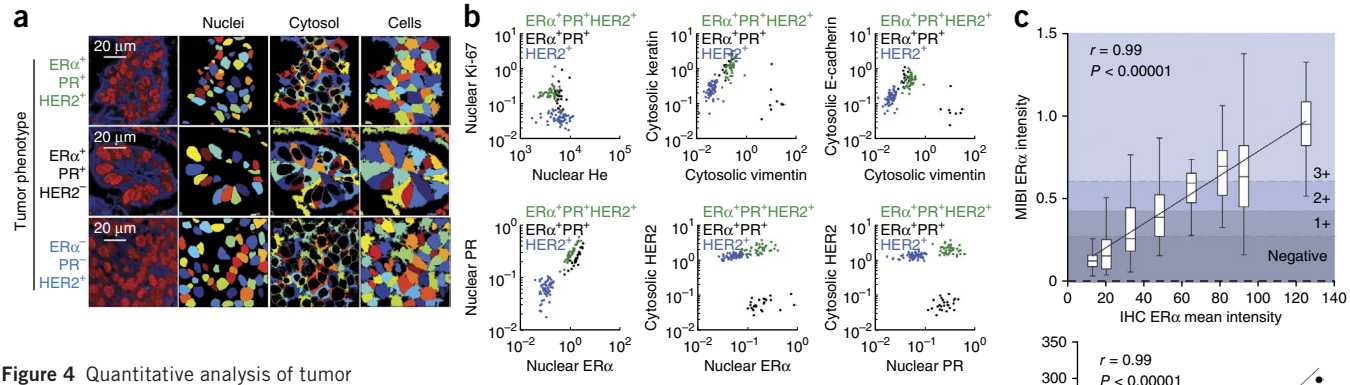

Figure 4 Quantitative analysis of tumor immunophenotype. (**a**) Image segmentation. Representative fields of view of breast tumor biopsies from three different patients segmented into nuclear and cytoplasmic regions of interest using dsDNA and hematoxylin channels. In total, twelve different breast tumor biopsies were analyzed with at least three replicates per biopsy. At least five fields of view were acquired for each replicate. (**b**) Feature extraction. Biaxial scatter plots illustrate quantitative expression patterns of each respective tumor. Each point represents the mean pixel intensity for each respective cell ROI. Biaxial plots are log scaled. He, hematoxylin. (**c**) Comparison of staining intensity using IHC and MIBI. ERα staining intensity of a cohort of nine breast tumors analyzed using IHC compared with corresponding values attained using MIBI. The distribution of single-cell staining intensity by MIBI as a function of the mean staining intensity by IHC is shown in a box-and-whisker plot. Lower and upper boundaries of each box are defined by the first and third quartiles, respectively. Whisker length is set to 1.5 times the interquartile range. Linear regression analysis comparing the mean intensities and H scores using the two methods are shown in the top and bottom graphs, respectively ($r = 0.99$, $P < 0.0001$, Student's t-test).

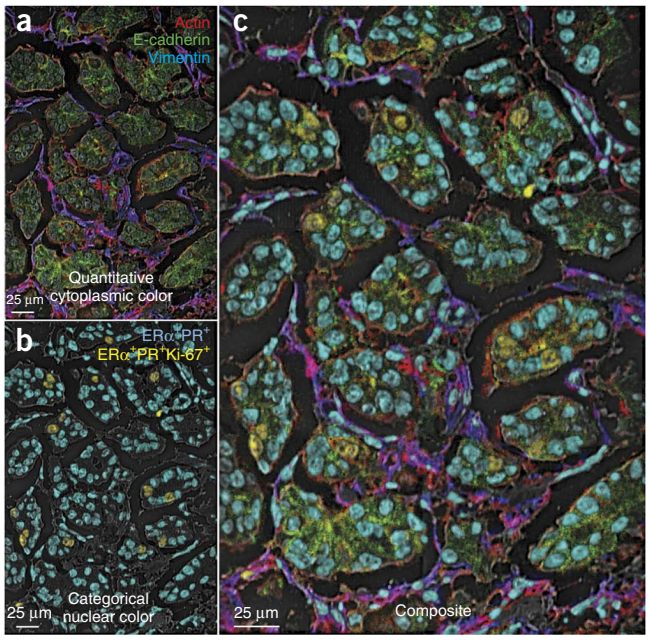

Figure 5 Composite representation of multidimensional MIBI data using categorical and quantitative colorization. (**a**) Quantitative colorization of cytoplasmic features. Three-color overlay of E-cadherin (green), actin (red) and vimentin (blue) channels serves as a quantitative representation of protein expression and colocalization. (**b**) Categorical colorization of nuclei. Subpopulations of ERα+PR+Ki-67+ or ERα+PR+ nuclei pseudocolored yellow or aqua, respectively. (**c**) Multidimensional data summarized in a composite image illustrating quantitative and categorical expression patterns. The composite is a representative image of twelve different breast tumor biopsies analyzed with at least three replicates per biopsy.

DISCUSSION

In this study, we have presented and validated elemental mass–based multiplexed IHC analysis that circumvents the limitations associated with conventional staining methods reliant on optical absorbance or fluorescence signals. This method can be used on virtually any vacuum-compatible specimen, including FFPE tissue. FFPE tissue is the most common type of specimen, with an estimated 1 billion blocks stored in clinical repositories globally[11]. In validating this method, we were able to demonstrate an immunophenotypic analysis of PBMCs that is almost quantitatively identical to that attained using mass cytometry. Subsequent multiplexed analyses FFPE breast tumor biopsies produced staining patterns and intensities for each antigen that were equivalent to validated, single-plex immunoperoxidase assays used in clinical labs. Additionally, marker multiplexing and image segmentation permitted quantitative feature extraction describing cellular and subcellular expression, which, in aggregate, revealed immunophenotypes of cell subpopulations that could be related back to the original clinical pathology of the tissue. We demonstrated the quantitative accuracy of MIBI via side-by-side comparison with an FDA-approved QIA IHC platform. Lastly, new approaches in combinatorial false (or pseudo-) coloring were used to distill pertinent high-dimensional features down to a rapidly interpretable image where multiple phenotypes are delineated using single colors.

MIBI has a number of advantages over conventional IHC techniques. Background signal due to autofluorescence is absent, and the five-log dynamic range presented here exceeds that of immunofluorescence and chromogenic IHC by 100-fold and 1,000-fold, respectively[2,20,21]. Because the mass accuracy can resolve less than a fraction of a dalton at even the lowest resolution (**Supplementary Fig. 3**), no spectral overlap is observed between mass-adjacent elemental reporters. Moreover, the reporter panel can be designed such that neither residual isotopic contaminants (**Supplementary Fig. 3** and **Supplementary Table 1**) nor metal oxide abducts (**Supplementary Figs. 4** and **5**) interfere materially with the reporter masses associated with each antibody probe, obviating the need for channel compensation in the experiments herein. The assay's linearity is better than that of both chromogenic IHC and immunofluorescence because neither secondary labeling nor amplified detection are required[2]. As relatively conventional methods are used for immunoreactions and because mass tags do not degrade, samples are stable indefinitely, permitting remote preparation together with a centralized reading facility.

Immunofluorescence-based multiplexing assays have been reported previously. Multispectral imaging with careful selection of antibodies, secondary antibodies, fluorescent dyes and filter cubes can be used to achieve multiplexing of up to seven simultaneous labels, although such performance is rarely achieved and requires much optimization[22]. Sequential methods for multiplexing, sometimes referred to as dye cycling, have been described that use the general approach of repeated cycles of primary staining (with or without secondary staining), imaging and then quenching or bleaching or otherwise removing each cycle's fluorescent reporters. Methods for erasing the signals have included low-pH antibody elutions, high-temperature fluorophore denaturation, antibody stripping or photobleaching[23–28]. These approaches have several shortcomings not found with MIBI. Some methods of dye cycling lead to accumulative structural changes that alter epitope antigenicity[23]. The techniques typically use just a few primary antibodies per round of staining, making the iterative methodology labor intensive and time consuming. Repeated processing of tissue sections can lead to altered histology that reduces the accuracy of image co-registration across staining cycles. In contrast, samples prepared for MIBI are stained with all antibodies in a single step. Markers are acquired in parallel in a single imaging session without any additional sample processing. Furthermore, histological stains, such as hematoxylin, are also detectable with this technique and can be overlaid with antibody expression data, making the representations created here indistinguishable from those of conventional IHC-based pathological analyses.

Other mass-based reporter systems have been used to image FFPE tissues previously[29]. These have taken two forms: matrix-assisted laser desorption ionization mass spectrometry (MALDI-MS) and laser-ablation inductively coupled plasma mass spectrometry (LA-ICP-MS). MALDI-MS imaging, although adept at analyzing macromolecules, has inherent limitations owing to its requirement for a crystalline chemical matrix[30–32]. The matrix, combined with the instrument sensitivity, reduces achievable resolution (>5 μm) and obscures the signal from elemental reporters. LA-ICP-MS imaging, on the other hand, offers many of the same benefits as MIBI (for example, dynamic range and multiplexing of isotopic reporters). However, laser spot size and instrument sensitivity in previous studies have been limited in elemental reporter–based imaging assays. As such, imaging studies of FFPE breast carcinomas using commercially available LA-ICP-MS systems have yielded images with around 100-μm resolution[33]—a factor of nearly three orders of magnitude greater than the 200- to 300-nm resolution achieved in the analysis presented here. Taken together, the complexity, sensitivity and resolution of previously reported mass-based techniques limit their deployment in a clinical setting.

One obstacle to broader application of MIBI is sample throughput. For antigens expressed at levels similar to those analyzed here, a 100-μm field of view for seven antibodies at a resolution comparable to that of light microscopy (200–300 nm) can be acquired in as little as 5 min. At this rate, a 500-μm field of view would require approximately 2 h to image. Larger numbers of antibodies could be acquired with repeat scans; however, this would increase the scan time proportionally. In future work, we expect to ameliorate the majority of these issues by employing newly developed primary ion beam sources and new instrument configurations. Next-generation oxygen ion sources with higher current densities and 50-nm beam spot sizes have recently become commercially available, theoretically permitting ~20-fold faster image acquisition than that of the current implementation described here[34]. This new ion beam source will provide lateral resolution comparable to that of confocal microscopy and axial resolution that exceeds confocal microscopy's[34]. Furthermore, new instrument configurations using a time-of-flight mass analyzer would permit parallel quantification of all mass reporters in a given experiment without a cyclic analysis. Taken together, gains from these achievable next-generation instrument configurations should reduce the acquisition time for 50–100 targets (mass reporters) in a 500-μm field of view to 5–10 min when imaged at resolutions equal to light microscopy.

In addition to instrument improvements, similar performance gains can be realized by increasing the amount of metal attached to each antibody. Current lanthanide metal antibody conjugation protocols achieve labeling efficiencies of 100–200 metal atoms per antibody[8]. The development of new nanoparticle-based reagents is projected to enable the attachment of up to 10,000 metal atoms per antibody. Such gains in labeling efficiency could further reduce scan times by as much as two orders of magnitude, such that a tumor microarray containing 1,000 600-μm core specimens could be imaged in as little as 1.5 h.

As a consequence of using antibodies for protein detection, MIBI inherits many of the issues that can limit the utility of conventional IHC. Poorly characterized reagents can exhibit nonspecific binding, and some epitopes are difficult to target with antibody-based approaches. However, we expect that reagents can be developed that will extend the capability of MIBI beyond antibody-based analysis to other arenas, such as *in situ* hybridization and subcellular metabolic analysis. These extended applications of MIBI, taken with the gains permitted by relatively minor modifications of existing analytical systems, introduce the prospect of a practical multiplexed imaging platform that integrates tissue histology, protein expression, gene expression and metabolism on a subcellular level. The basic science utility of such a system is evident, and clinical deployment of this technology would extend multiplexed expression analysis typically restricted to flow cytometry of cell suspensions (such as blood) to any solid tissue. Given the transformative effect that flow cytometry has shown in the diagnosis, staging and treatment of hematopoietic malignancies, the present approach, when applied to solid tissue samples, could provide new insight into disease pathogenesis, address pathway activation status, explore tumor heterogeneity and document effects of therapeutic interventions that could ultimately improve patient outcomes.

METHODS

Methods and any associated references are available in the online version of the paper.

Note: Any Supplementary Information and Source Data files are available in the online version of the paper.

ACKNOWLEDGMENTS

We thank N. Hubbard, C. Espiritu, S. Rost, L. Rangell and the Genentech Human Tissue Lab for assistance in preparing and processing tissue sections. We also thank A. Jager for technical support with CyTOF and antibody labeling. M.A. is supported by the Stanford Molecular Imaging Scholars Program through the US National Institutes of Health (NIH, 5R25CA11868107). S.C.B. is supported by the Damon Runyon Cancer Research Foundation Fellowship (DRG-2017-09) and NIH (1K99 GM104148-01). R.F. is supported by Northrop-Grumman Corporation (7500108142 BISC). This work was supported by a US National Science Foundation equipment grant (0922648) to the Stanford Nano Center for the NanoSIMS 50L analytical system used in the work here. This work was also supported by grants (to the Nolan lab) from the NIH (0158 G KB065, 1R01CA130826, 5U54CA143907, HHSN272200700038C, N01-HV-00242, 41000411217, 5-24927, P01 CA034233-22A1, P01 CA034233-22A1, PN2EY018228, RFA CA 09-009, RFA CA 09-011, U19 AI057229 and U54CA149145), the California Institute for Regenerative Medicine (DR1-01477 and RB2-01592), the European Commission (HEALTH.2010.1.2-1), the US FDA (HHSF223201210194C: BAA-12-00118), the US Department of Defense (W81XWH-12-1-0591 OCRP-TIA NWC) and the Entertainment Industry Foundation.

AUTHOR CONTRIBUTIONS

M.A., S.C.B. and R.F. conducted experiments and wrote the manuscript. M.B.H. designed and fabricated reagents. C.H. assisted in data acquisition and experimental design. A.D.B. and R.M.L. prepared tissue sections, performed IHC and assisted in writing the manuscript. J.B.L., S.D.L., S.Z. and Y.N. prepared tissue sections, performed IHC and assisted in optimizing protocols used in MIBI analysis. G.P.N. assisted in experimental design and wrote the manuscript.

COMPETING FINANCIAL INTERESTS

The authors declare competing financial interests: details are available in the online version of the paper.

1. Coons, A.H., Creech, H.J., Jones, R.N. & Berliner, E. The demonstration of pneumococcal antigen in tissues by the use of fluorescent antibody. *J. Immunol.* **45**, 159–170 (1942).
2. Rimm, D.L. What brown cannot do for you. *Nat. Biotechnol.* **24**, 914–916 (2006).
3. Anagnostou, V.K. *et al.* Analytic variability in immunohistochemistry biomarker studies. *Cancer Epidemiol. Biomarkers Prev.* **19**, 982–991 (2010).
4. Bordeaux, J. *et al.* Antibody validation. *Biotechniques* **48**, 197–209 (2010).
5. McCabe, A., Dolled-Filhart, M., Camp, R.L. & Rimm, D.L. Automated quantitative analysis (AQUA) of in situ protein expression, antibody concentration, and prognosis. *J. Natl. Cancer Inst.* **97**, 1808–1815 (2005).
6. Hasui, K. *et al.* Double autoimmunostaining with glycine treatment. *J. Histochem. Cytochem.* **51**, 1169–1176 (2003).
7. Bendall, S.C. *et al.* Single-cell mass cytometry of differential immune and drug responses across a human hematopoietic continuum. *Science* **332**, 687–696 (2011).
8. Lou, X. *et al.* Polymer-based elemental tags for sensitive bioassays. *Angew. Chem. Int. Edn Engl.* **46**, 6111–6114 (2007).
9. Ornatsky, O.I. *et al.* Development of analytical methods for multiplex bio-assay with inductively coupled plasma mass spectrometry. *J. Anal. At. Spectrom.* **23**, 463–469 (2008).
10. Ornatsky, O. *et al.* Highly multiparametric analysis by mass cytometry. *J. Immunol. Methods* **361**, 1–20 (2010).
11. Bandura, D.R. *et al.* Mass cytometry: technique for real time single cell multitarget immunoassay based on inductively coupled plasma time-of-flight mass spectrometry. *Anal. Chem.* **81**, 6813–6822 (2009).
12. Blow, N. Tissue preparation: tissue issues. *Nature* **448**, 959–963 (2007).
13. Lechene, C. *et al.* High-resolution quantitative imaging of mammalian and bacterial cells using stable isotope mass spectrometry. *J. Biol.* **5**, 20 (2006).
14. Senyo, S.E. *et al.* Mammalian heart renewal by pre-existing cardiomyocytes. *Nature* **493**, 433–436 (2013).
15. Steinhauser, M.L. *et al.* Multi-isotope imaging mass spectrometry quantifies stem cell division and metabolism. *Nature* **481**, 516–519 (2012).
16. Williams, P. Biological imaging using secondary ions. *J. Biol.* **5**, 18 (2006).
17. Gordon, A. *et al.* Single-cell quantification of molecules and rates using open-source microscope-based cytometry. *Nat. Methods* **4**, 175–181 (2007).
18. Carpenter, A.E. *et al.* CellProfiler: image analysis software for identifying and quantifying cell phenotypes. *Genome Biol.* **7**, R100 (2006).
19. Kamentsky, L. *et al.* Improved structure, function and compatibility for CellProfiler: modular high-throughput image analysis software. *Bioinformatics* **27**, 1179–1180 (2011).
20. Bodo, J., Durkin, L. & Hsi, E.D. Quantitative *in situ* detection of phosphoproteins in fixed tissues using quantum dot technology. *J. Histochem. Cytochem.* **57**, 701–708 (2009).

21. Camp, R.L., Chung, G.G. & Rimm, D.L. Automated subcellular localization and quantification of protein expression in tissue microarrays. *Nat. Med.* **8**, 1323–1327 (2002).
22. Tsurui, H. *et al.* Seven-color fluorescence imaging of tissue samples based on Fourier spectroscopy and singular value decomposition. *J. Histochem. Cytochem.* **48**, 653–662 (2000).
23. Glass, G., Papin, J.A. & Mandell, J.W. SIMPLE: a sequential immunoperoxidase labeling and erasing method. *J. Histochem. Cytochem.* **57**, 899–905 (2009).
24. Wählby, C., Erlandsson, F., Bengtsson, E. & Zetterberg, A. Sequential immunofluorescence staining and image analysis for detection of large numbers of antigens in individual cell nuclei. *Cytometry* **47**, 32–41 (2002).
25. Pirici, D. *et al.* Antibody elution method for multiple immunohistochemistry on primary antibodies raised in the same species and of the same subtype. *J. Histochem. Cytochem.* **57**, 567–575 (2009).
26. Friedenberger, M., Bode, M., Krusche, A. & Schubert, W. Fluorescence detection of protein clusters in individual cells and tissue sections by using toponome imaging system: sample preparation and measuring procedures. *Nat. Protoc.* **2**, 2285–2294 (2007).
27. Schubert, W. *et al.* Analyzing proteome topology and function by automated multidimensional fluorescence microscopy. *Nat. Biotechnol.* **24**, 1270–1278 (2006).
28. Schubert, W., Gieseler, A., Krusche, A. & Hillert, R. Toponome mapping in prostate cancer: detection of 2000 cell surface protein clusters in a single tissue section and cell type specific annotation by using a three symbol code. *J. Proteome Res.* **8**, 2696–2707 (2009).
29. Wu, B. & Becker, J.S. Imaging of elements and molecules in biological tissues and cells in the low-micrometer and nanometer range. *Int. J. Mass Spectrom.* **307**, 112–122 (2011).
30. Seeley, E.H. & Caprioli, R.M. Imaging mass spectrometry: Towards clinical diagnostics. *Proteomics Clin. Appl.* **2**, 1435–1443 (2008).
31. Aerni, H.-R., Cornett, D.S. & Caprioli, R.M. High-throughput profiling of formalin-fixed paraffin-embedded tissue using parallel electrophoresis and matrix-assisted laser desorption ionization mass spectrometry. *Anal. Chem.* **81**, 7490–7495 (2009).
32. Caprioli, R.M. Perspectives on imaging mass spectrometry in biology and medicine. *Proteomics* **8**, 3679–3680 (2008).
33. Giesen, C. *et al.* Multiplexed immunohistochemical detection of tumor markers in breast cancer tissue using laser ablation inductively coupled plasma mass spectrometry. *Anal. Chem.* **83**, 8177–8183 (2011).
34. Smith, N.S., Tesch, P.P., Martin, N.P. & Kinion, D.E. A high brightness source for nano-probe secondary ion mass spectrometry. *Appl. Surf. Sci.* **255**, 1606–1609 (2008).

ONLINE METHODS

Substrate preparation. Silicon wafers (Silicon Valley Microelectronics) were diced into 18-mm^2 pieces, rinsed two times with methanol and polished with a cotton-tipped applicator. Cleaned substrates were subsequently immersed in 2% poly-L-lysine solution (Sigma-Aldrich) for 10 min and baked at 60 °C for 1 h.

Antibodies. A summary of antibodies, reporter isotopes and concentrations can be found in **Supplementary Tables 1** and **2**. Metal-conjugated primary antibodies were prepared 100 µg at a time using the MaxPAR antibody conjugation kit (DVS Sciences, Toronto, Canada) according to the manufacturer's recommended protocol. Following labeling, antibodies were diluted in Candor PBS Antibody Stabilization Solution (Candor Bioscience GmbH, Wangen, Germany) to 0.4 mg mL^{-1} and stored long-term at 4 °C.

Cells. Unmatched human peripheral blood was purchased from the Stanford Blood Bank with approval from the Stanford University Institutional Review Board. All blood samples were collected in heparan sulfate anticoagulant, stored at room temperature for 4–6 h and then separated over Ficoll-Paque PLUS (Amersham Biosciences) using ACCUSPIN Tubes (Sigma-Aldrich, St. Louis, MO) to remove erythrocytes, platelets and granulocytes. Cells were frozen in FCS with 10% DMSO. Cells were rested at 37 °C, 5% CO_2 for 1 h in RPMI with 10% FCS (supplemented with 2 mM EDTA in the case of frozen samples), 1× L-glutamine and 1× penicillin with streptomycin (Invitrogen).

Staining of peripheral blood mononuclear cells. Cellular staining protocols were based on procedures previously described. Briefly, after resting cells for 1 h, surface marker antibodies were added yielding 100-µL final reaction volumes and incubated at room temperature for 30 min. Following incubation, cells were washed two times with cell-staining medium and split into two aliquots. For mass cytometry analysis, cells were permeabilized with 4 °C methanol for 10 min at 4 °C, washed twice with cell-staining medium to remove residual methanol and then stained with 1 mL of 1:4,000 ^{191,193}Ir DNA intercalator diluted in PBS with 1.6% PFA for 20 min at room temperature. Cells were then washed once with cell-staining medium, once with PBS and then diluted in distilled water (dH_2O) to approximately 1×10^6 cells per milliliter before analysis. For MIBI analysis, 50 µL of cells diluted in PBS to approximately 1×10^7 cells per milliliter were placed on silicon substrate and allowed to adhere for 20 min. The substrate was then gently rinsed with PBS, fixed for 5 min in PBS with 2% glutaraldehyde and rinsed twice with dH_2O. Lastly, samples were dehydrated via a graded ethanol series, air dried at room temperature and stored in a vacuum desiccator for at least 24 h before analysis.

Breast tumor tissue sections. Tissue sections (4-µm thickness) were cut from FFPE tissue blocks of archival deidentified human breast tumor biopsies from UC Davis or Genentech using a microtome and mounted on poly-L-lysine–coated silicon substrate for MIBI analysis or a glass slide for immunoperoxidase staining. Silicon-mounted sections were baked at 65 °C for 15 min, deparaffinized in xylene and rehydrated via a graded ethanol series. The sections were then immersed in epitope retrieval buffer (10 mM sodium citrate, pH 6) and placed in a pressure cooker for 30 min (Electron Microscopy Sciences, Hatfield, PA). The sections were subsequently rinsed twice with dH_2O and once with wash buffer (TBS, 0.1% Tween, pH 7.2). Residual buffer was removed by gently touching the surface with a lint-free tissue before incubating with blocking buffer for 30 min (TBS, 0.1% Tween, 3% BSA, 10% donkey serum, pH 7.2). Blocking buffer was subsequently removed, and the sections were stained overnight at 4 °C in a humidified chamber. The following morning, the sections were rinsed twice in wash buffer, postfixed for 5 min (PBS, 2% glutaraldehyde), rinsed in dH_2O and stained with Harris hematoxylin for 10 s. Finally, the sections were dehydrated via graded ethanol series, air dried at room temperature and then stored in a vacuum desiccator for at least 24 h before imaging. For immunoperoxidase staining, antigen retrieval was performed using a Decloaking Chamber (Biocare Medical, Concord, CA) with citrate buffer at pH 6.0, 125 °C and pressure to 15 p.s.i. The total time slides were in the chamber was 45 min. Incubations with primary antibodies were performed at room temperature overnight in a humidified chamber. Normal goat serum was used for blocking. Biotinylated goat anti-rabbit (1:1,000 titer, polyclonal, Vector Labs, Burlingame, CA) was the secondary antibody used with a Vectastain ABC Kit Elite and with a Peroxidase Substrate Kit DAB (Vector Labs, Burlingame, CA) for amplification and visualization of signal, respectively. Tissues known to contain each assessed antigen were used as positive controls.

Multiplexed ion beam imaging analysis. MIBI analysis was performed with a NanoSIMS 50L mass spectrometer (Cameca) using an O^- primary ion beam supplied by an oxygen duoplasmatron source. The primary optics, secondary optics and mass spectrometer were tuned before each experiment. The seven detector trolleys were tuned to the elemental peak corresponding to each metal isotope–conjugated antibody using antibody master mixes that had been air dried on silicon. Images containing more than seven channels were acquired by recalibrating the detector trolleys between repeat scans of the same field. The detectors were tuned to the following masses for the first imaging cycle: detector 1, ^{27}Al; detector 2, ^{139}La; detector 3, ^{143}Nd; detector 4, ^{147}Sm; detector 5, ^{158}Gd; detector 6, ^{166}Er; and detector 7, ^{176}Yb. The following settings were used for the second imaging cycle: detector 4, ^{154}Sm; detector 5, ^{162}Dy; and detector 6, ^{168}Er. All data were taken in positive-ion mode using D1 aperture 2, D0 aperture 0 or 3 and L1 voltage of approximately 1,500 V. Because resolving the metal isotopes of interest requires only unit resolution, entrance slit 0 and aperture slit 0 were used in order to maximize ion transmission to the detectors (**Supplementary Figs. 1** and **2**). ROIs identified on serial sections using brightfield microscopy were located using the charge-coupled device camera in the NanoSIMS analysis chamber. Ion images were acquired for fields of view from 50 to 100 µm with pixel dwell times between 2 and 10 ms, with up to ten repeat scans over a single area. Total scan time for a single field of view ranged between 5 and 25 min. Larger areas were constructed by stitching together multiple contiguous fields of view into a single mosaic.

Mass cytometry measurement. Cell events were collected on a CyTOF mass cytometer as previously described[6]. With detection in dual-counting mode using the 'data' calibration, event length was set to range from 10 to 75 pulses with a convolution threshold of 100. A detector stability delay of 20 s was used, and all samples were diluted such that the acquisition rate was less than 500 cells per second.

Peripheral blood mononuclear cell mosaic stitching. The MIBI PBMC data were collected in a series of 1,200 individual square 50-µm (128 pixel) tiles, arranged in a 40 × 30 rectangle. The relative positions of the tiles were determined using the log-transformed CD45 images. The reported offset between adjacent tiles was 40 µm in both the *x* and *y* directions, but the actual offset was observed to vary owing to imprecision in the stage's location. To account for this, each tile was initially placed according to its reported offset and then moved ~1–20 pixels in both the *x* and *y* directions to multiple different positions. At each location, the correlation in the overlap area between the new tile and previous tile was computed. The tile was then assigned to the position that maximized the correlation of the overlapped areas.

Peripheral blood mononuclear cell image segmentation. The log-transformed mosaic of CD45 tiles was convolved with a two-dimensional Gaussian kernel with s.d. of 3 pixels. A threshold at a density of one count was applied. Each continuous region with density greater than this threshold was preliminarily labeled as an individual cell. The next step was to separate into their constituent singlets any sets of multiple cells that were close enough to be initially labeled as single cells. To do this, for each preliminary cell, the two points on the boundary were identified between which there was the maximum ratio of distance along the boundary to Euclidean distance (the 'pinch points'). When this ratio exceeded 0.42 (a heuristic cutoff), the preliminary cell was separated into two cells with a new border segment between the pinch points. This process was repeated for all cells and then repeated with each new preliminary cell created, until no cells had pinch points that exceeded this separation criteria[17].

Once the cell boundaries were determined, the raw values of each channel measured were summed within each boundary to create a table of total ion intensity on a per-cell basis. The number of pixels within each cell was also

calculated as a measure of cell size. This table was equivalent to an .fcs file similar to that from a standard mass cytometry experiment.

Statistical analyses. To filter out doublets and debris, singlets were gated from the mass cytometry PBMCs by applying standard event length by DNA and then event length by CD45 gates; a singlet gate using cell area (total pixels per cell) by CD45 was applied to the MIBI PBMCs. The subsequent gating scheme for both the MIBI- and CyTOF-processed PBMCs is shown in **Figure 2** panels **b** and **c**, respectively. No statistical method was used to predetermine sample size.

doi:10.1038/nm.3488